Applied Surface Science 502 (2020) 144288

Contents lists available at ScienceDirect

Applied Surface Science

journal homepage: www.elsevier.com/locate/apsusc

Full Length Article

# Synergistic photoelectrochemical performance of La-doped $RuO_2$-$TiO_2$/Ti electrodes

Juan Zuo[a,b], Junqiu Zhu[c], Mingzhou Zhang[a], Qiming Hong[d], Jie Han[e], Jianfu Liu[b,*]

[a] Fujian Provincial Key Laboratory of Functional Materials and Applications, Xiamen University of Technology, Xiamen 361005, PR China
[b] Fujian Engineering and Research Center of Rural Sewage Treatment and Water Safety, Xiamen University of Technology, Xiamen 361005, PR China
[c] College of Chemical Engineering and Materials Science, Quanzhou Normal University, Quanzhou, Fujian 362000, China
[d] Xiamen University, Xiamen, Fujian 361005, China
[e] School of Science & Technology, Open University of Hong Kong, Kowloon, Hong Kong SAR, PR China

ARTICLE INFO

*Keywords:*
Photoelectrochemical effect
La doping
$RuO_2$-$TiO_2$/Ti electrode
Dye degradation
Thin films
Functional

ABSTRACT

$RuO_2$-$TiO_2$/Ti electrodes with low-content La-doping are prepared by thermal decomposition method. The effect of La doping on their electrochemical performance upon UV illumination are investigated. The doped electrodes show higher density of cracks and rugosity in microscale on the surface than the undoped ones. They also have a negative shift of the onset potential of oxygen evolution from 1.1 V to 1.0 V and higher current intensity under UV irradiation as well. Electrochemical impedence spectroscopy analysis demonstrates a better electrical conductivity of the doped film. Electron paramagnetic resonance results show that the obtained La-doped $TiO_2$ surface provides a higher density of oxygen vacancies. This anode also has 7.5% higher degradation rate of the methylene blue than La-undoped ones under UV irradiation. This is probably due to the increased surface rugosity and better electric conductivity, higher density of oxygen vacancies under UV irradiation by the doping of La ions.

## 1. Introduction

Dimensionally stable anode (DSA) coating is composed of a mixture of Ti and Ru oxides. $RuO_2$ and $TiO_2$ are isomorphic with similar metal ionic radius and hence they can exist stably in the same crystal lattice and form $Ti_{1-x}Ru_xO_2$ oxides or solid solutions with the same grain size. DSA has been developed for the chlorine and oxygen generation in the industry due to its excellent electrocatalytic properties and mechanical and chemical stability. It is also used to degrade organic dyes solutions when applying an electric field and/or exposed to UV light. The photocatalysis and electrolysis occur synergistically on the electrode surface leading to an increase in the degradation rate of dye solutions. However, it shows a limited oxidation power for degrading dyes due to its low ability to electrogenerate hydroxyl radicals [1].

$RuO_2$ plays a role to increase the metallic conductivity and electrocatalytic activity of the anode, whereas $TiO_2$ is photochemically active semiconductor. DSA with the higher amount of $TiO_2$ shows higher stability but lower electrocatalytic activity and electrical conductivity with respect to $RuO_2$ under the electrochemically oxidative conditions. A lot of work has been done to study the effect of Ti:Ru ratio in a systematic way on their electrocatalytic activity and electrical conductivity [2-4]. The maximum activity towards chlorine evolution with a composition of around $Ru_{0.3}M_{0.7}O_2$ is referred to DSA.

The outer electron configuration of Ru is $4d^75s^1$, when it gives four electrons to two adjacent oxygen atoms to form the covalent bond, there are still 4 left electrons not involved in the shared movement. This makes the bandgap of the coating decreasing from 3.2 eV of pure $TiO_2$ to almost 0.2 eV with the addition of $RuO_2$. $Ru^{4+}$ is also a strong positive electric center due to the migration of free electrons in the coating under a positive electric field. These sites are the active sites for the electrocatalytic activities. When this solid solution is deficient of oxygen, the free electrons increase to 6 N from 4 N and hence the electrocatalytic activities increases as well. Some of the metal ions have been added to increase their electrocatalytic activities such as Ni [5], Co [6], Zn [7], and Sb [8] in either $RuO_2$ or along with Ru in $TiO_2$. These transition metal elements with higher number of d-electrons compared to Ru have lower valent and improve the electrocatalytic activity owing to an improved electronic charge transport caused by higher conductivity due to formation of oxygen vacancies [9].

In addition, the light with a photon energy larger than the band gap of $TiO_2$ can reduce $Ti^{4+}$ to $Ti^{3+}$ and generates oxygen vacancies at oxygen bridge sites as well [10-12]. The formation of oxygen vacancies

* Corresponding author.
*E-mail address:* liujf@xmut.edu.cn (J. Liu).

https://doi.org/10.1016/j.apsusc.2019.144288
Received 28 August 2019; Received in revised form 30 September 2019; Accepted 4 October 2019
Available online 09 October 2019
0169-4332/ 

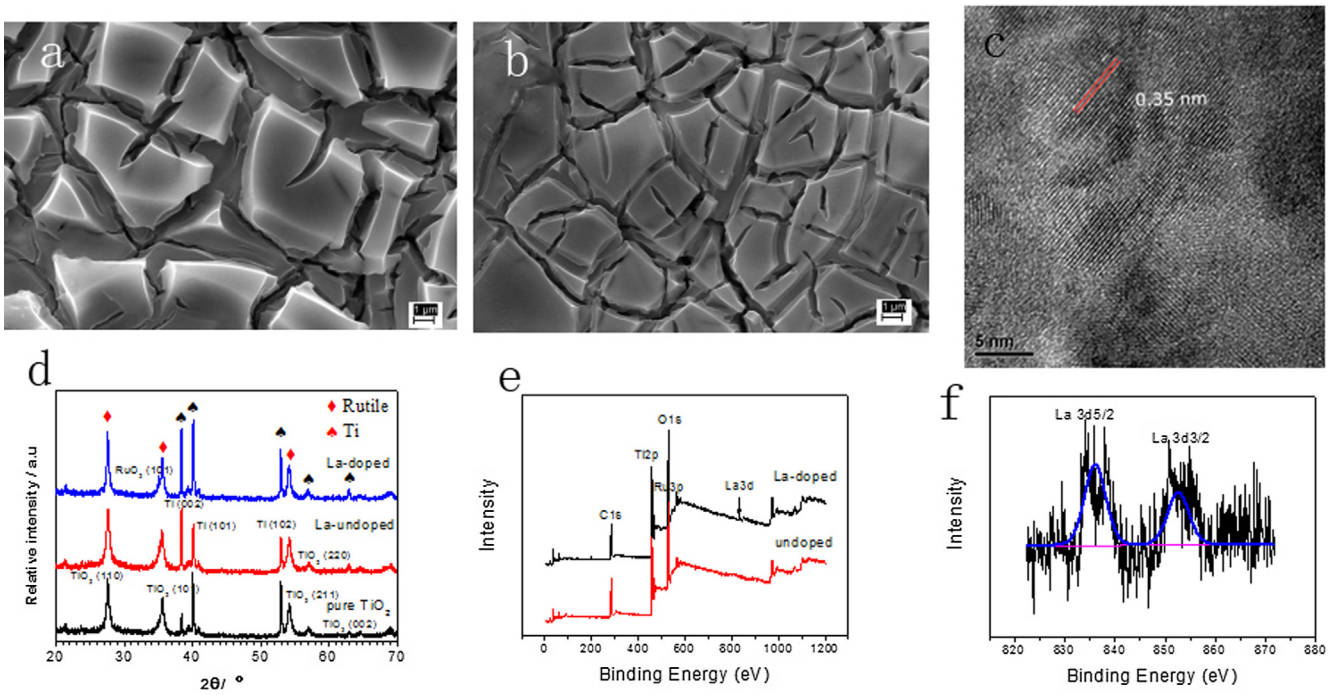


**Fig. 1.** (a) and (b) SEM images of $RuO_2$-$TiO_2$/Ti (a) and La-doped $RuO_2$-$TiO_2$/Ti electrodes (b). (c) HRTEM image of La-doped $RuO_2$-$TiO_2$/Ti electrode. (d) XRD pattern of La-doped $RuO_2$-$TiO_2$/Ti electrode. (e) XPS spectra of La-undoped and La-doped $RuO_2$-TiO2/Ti electrode. (f) Deconvoluted XPS spectrum of La element of La-doped $RuO_2$-$TiO_2$/Ti electrode.

at the two coordinated bridging sites of the $TiO_2$ upon UV illumination are favorable sites for dissociative dye and water adsorption and gave rise to the dissociative adsorption of dye molecules [13]. The photoelectrocatalytic activities of the coating is closely related to the content of oxygen vacancies in the coating as well [2,14].

The above-mentioned phenomena provide heuristics for the preparation of composite coatings with a certain amount of oxygen vacancies under electric field and UV illumination. Rare earth metal dopants are reported to be able to enhance the electrocatalytic and photocatalytic activities of $TiO_2$ coating [15], though there are still controversy about the enhancement mechanism. Among the suitable dopant for DSA system, La is a good candidate because its low-valent doping results in the formation of oxygen vacancies on the exterior or surface lattice and hence improves the electrocatalytic activity[9]. Some La ions are also believed to be able to extend the absorption to visible light spectrum of $TiO_2$ [16]. Choi et al., however, reports unchanged absorption spectrum for La-doped $TiO_2$ [17]. Zhang et al. find that La-doped $TiO_2$ photoanode can provide a higher density of oxygen vacancies on the surface and thus result in higher dyes absorption in dye-sensitized solar cells [18]. It is believed when doping with La into photosensitive $TiO_2$ film will enhance its photocatalytic performance upon UV irradiation [19]. It is also found that the anatase-to-phase transformation of $TiO_2$ can be inhibited and the thermal stability of its mesoporous structures is remarkably improved by La doping as well [20]. Murakami et al. report the lanthanum chlorides was the effective pore initiators in the preparation of porous La-doped $RuO_2$/Ti (Ru:La = 7:3) electrodes due to the large ionic radium of La [21].

However, few studies about the effect of low-content La-doping on the $RuO_2$-$TiO_2$/Ti electrodes have been reported. In this work, a low content of La ions were doped on the $RuO_2$-$TiO_2$/Ti electrodes and their effect on the film structure, performance as anode on the oxygen evolution and degradation of methylene blue solution under UV irradiation were investigated.

## 2. Experimental

La-doped $RuO_2$-$TiO_2$/Ti electrodes were prepared by thermal decomposition method. 1 mol/L $RuCl_3 \cdot xH_2O$, 1 mol/L tetrabutyl titanate and 0.1 mol/L lanthanum nitrate in anhydrous ethanol were mixed in an atomic concentration of Ti:Ru:La = 7:3:0.3. The mixed solutions were then painted on the etched Ti substrates, dried at 100 °C for 3 min under infrared light, and then calcinated in a furnace at 450 °C for 10 min for several times until the solution were finished. Finally, these samples were annealed at 500 °C for 1 h. The film morphology were observed by field emission SEM (SEM, Hitachi, S4800) and high resolution transmission electron microscope HRTEM (Tecnai F30, Philips-FEI). X-ray diffraction (XRD) pattern was performed with Philips. Xpert-MPD X. X-ray photoelectron spectra (XPS) were obtained using Quantum 2000, Physical Electronics, USA. The electron paramagnetic resonance investigation was performed by using a Bruker EMX-10/12 spectrometer under light irradiation (Xenon lamp 300 W, PLS-SXE300C Beijing Perfectlight Technology Co., Ltd.) at room temperature under an ambient atmosphere and UV irradiation. Before measurements, the samples were illuminated for about 1 min. The electrochemical measurements were done by the electrochemical workstation (CHI 760). The as-prepared electrodes were used as the working electrode, a saturated calomel electrode (SCE) and a platinum sheet served as the reference electrode and counter electrode, respectively. A UV cold cathode lamp (ca 6 μm/cm$^2$, Stanley electric CO., LTD.) was inserted into the center of the solution as the UV irradiation source. The polarization curves were scanned at the rate of 5 mV/s in 0.1 mol/L $Na_2SO_4$ solution. Electrochemical impedence spectroscopy (EIS) tests were carried out obtained at 1.4 V in the presence of 0.1 M $Na_2SO_4$ solution for frequencies ranging from $10^5$ Hz to $10^0$ Hz. The fitting of the measured data was performed with Zsimpwin software. The degradation reaction of 100 mL of 0.1 mol/L $Na_2SO_4$ and 10 mg/L methylene blue solution was done in a electrochemical cell with quartz windows using a Pt sheet as counter electrode. A direct current of 11 mA/cm$^2$ was applied to the anode. After 5 min, 2 mL solution was taken and its absorption spectra were measured with UV–vis

spectrometer (DRS, Varian, Cary 5000). The photodegradation rate (PA) was calculated according to this equation, $PA = \frac{\text{Initial absorbance - Aborbance after degradation}}{\text{Initial absorbance}} \times 100\%$. The absorbance values were taken at 664 nm of methylene solution absorption spectra.

## 3. Results and discussion

Fig. 1(a) and (b) show the typical SEM images of $RuO_2$-$TiO_2$/Ti and La-doped $RuO_2$-$TiO_2$/Ti electrodes. Both samples exhibit the typical dried cracked mud characteristics. These appearances are caused by thermal shocks during solvent evaporation and calcination. These muds are flat, rather than the mesoporous structure of La-doped coating at a relatively high content of La [21]. The number of La-doped $RuO_2$-$TiO_2$/Ti cracks is higher than the undoped one, which demonstrates a higher rugosity in microscale. X-ray diffraction pattern of La-doped $RuO_2$-$TiO_2$/Ti sample shows that no crystalline $La_2O_3$ phase forms in the coatings (in figure (d)) due to a low level doping of La. XPS investigation (as shown in Fig. 1(e) and (f)) confirms that La have been doped into the surface of $RuO_2$-$TiO_2$/Ti samples with the addition of La ions. Fig. 1(c) shows the typical HRTEM image of La-doped $RuO_2$-$TiO_2$/Ti sample. The spacing between lattices in the crystal phase is 0.35 nm which corresponds to the lattice spacing of (1 0 1) of $TiO_2$. There is no evidence of crystalloid lanthanum oxide in the crystal which shows that La atom does not enter into the bulk lattice of $TiO_2$. Due to the disparity of the radius between $La^{3+}$(1.03 Å) and $Ti^{4+}$(0.745 Å), $Ru^{4+}$ (0.76 Å) [22], La ions can only be doped into the exterior or surface lattice in the form of Ti-O-La or La-O-La onto the surface of coatings instead of entering into the bulk lattice of $Ti_{1-x}Ru_xO_2$ [18].

Fig. 2(a) shows the linear sweep voltammetric curves of different samples. As a valve metal, Ti and $TiO_2$/Ti anode is barely conductive, even under UV irradiation as shown of curve (a) and (b). Curve (c) presents the typical anodic polarization behavior of the DSA electrodes. When the potential is lower than 1.1 V, the current intensity was almost constant due to charging the electrical double layer [23]. The electrochemical current increases rapidly originating from the oxygen evolution starting from 1.1 V. The La-doped $RuO_2$-$TiO_2$/Ti electrode (curve (d)) shows higher current intensity from 1.1 V than that of the undoped electrode (curve (c)). The surface cracks can provide the channels for the smooth release of oxygen gas bubbles [23]. The $RuO_2$-$TiO_2$/Ti electrode under UV irradiation (curve (e)) shows a negative shift of the onset potential to around 1.0 V and a higher current intensity from 1.0 V than that of the same electrode without UV irradiation. The La-doped $RuO_2$-$TiO_2$/Ti electrode under UV irradiation (curve (f)) shows a further negative shift and much higher current intensity. Fig. 2(b) is the the current intensity difference obtained by subtracting the curve (e) and curve (d) from the curve (f). Curve (a) indicates the effect of La ions doped into the electrode, which contributes the increase of current intensity. Curve (b) is the photocurrent of the La-doped $RuO_2$-$TiO_2$/Ti electrode, indicating a higher photocatalytic activity of the coating with the doping of La.

**Table 1**
Electrochemical parameters of different electrodes with and without UV irradiation simulated from the EIS analysis.

| | | $R_s$ | Q | n | $R_{ct}$ |
|---|---|---|---|---|---|
| Pure $TiO_2$ | | 3.025 | $6.5 \times 10^{-5}$ | 0.84 | 8112.2 |
| La-undoped | | 2.848 | $2.3 \times 10^{-4}$ | 0.75 | 579.8 |
| La-doped | | 2.004 | $7.8 \times 10^{-4}$ | 0.66 | 399.2 |
| UV irradiation | Pure $TiO_2$ | 3.103 | $6.5 \times 10^{-5}$ | 0.84 | 7386.4 |
| | La-undoped | 1.609 | $3.2 \times 10^{-4}$ | 0.73 | 565.6 |
| | La-doped | 1.707 | $1.3 \times 10^{-4}$ | 0.62 | 289 |

Fig. 2(c) and (d) shows the Nyquist plots of different electrodes without and with UV irradiation. The equivalent circuits $R_s(QR_{ct})$ in the inset are best fit to our experimental data [24]. $R_s$ represents the solution resistance, $R_{ct}$ the charge transfer resistance of a faradaic process occurring at the electrode/solution interface, and Q is the CPE (constant phase element), the double-layer capacitance of the electrode/solution interface. The fitted results are shown in Table 1. Due to the high bandgap value of $TiO_2$ semiconductor, pure $TiO_2$ electrodes show the highest $R_{ct}$ value as shown in Fig. 2(c), which is consisted with the linear sweep voltammetric measurements. The photogenerated hole-electron pairs in $TiO_2$ film once upon UV illumination contribute to the decrease of $R_{ct}$ value from 8112 to 7386 $\Omega cm^2$ [25]. The mixture of $RuO_2$ into $TiO_2$ films and the formation of solid solution further decrease the $R_{ct}$ due to the increase of the film conductivity. The La-doped

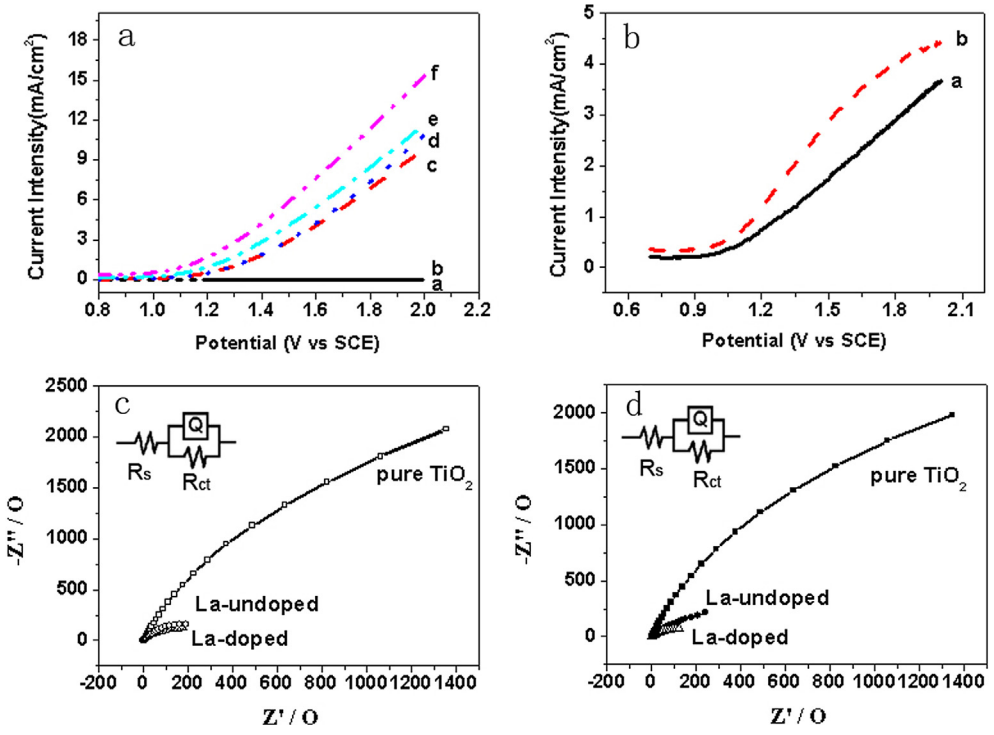


**Fig. 2.** (a) Linear sweep voltammetric curves of different electrodes: curve (a) pure $TiO_2$/Ti electrode, curve (b) pure $TiO_2$/Ti electrode under UV irradiation, curve (c) $RuO_2$-$TiO_2$/Ti electrode, curve (d) La-doped $RuO_2$-$TiO_2$/Ti electrode, curve (e) $RuO_2$-$TiO_2$/Ti electrode under UV irradiation, curve (f) La-doped $RuO_2$-$TiO_2$/Ti electrode under UV irradiation; (b) difference obtained by subtracting the curve (e) and curve (d) from the curve (f) in figure (a), which is curve (a) and (b) respectively. Curve (a) indicates the effect of La ions doped into the electrode. Curve (b) is the photocurrent of the La-doped $RuO_2$-$TiO_2$/Ti electrode, indicating a higher photocatalytic activity of the coating; (c) Nyquist plots of different electrodes; (d) Nyquist plots of different electrodes under UV irradiation. The insets are their simulating equivalent circuits.

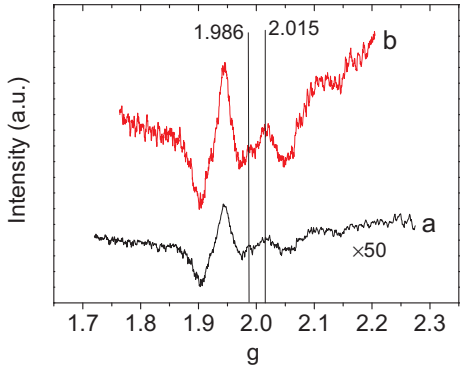


**Fig. 3.** The electron paramagnetic resonance spectra of (a) $RuO_2$-$TiO_2$/Ti electrode with 50 times magnification and (b) La-doped $RuO_2$-$TiO_2$/Ti electrode under UV irradiation.

**Table 2**
The photodegradation rate of methylene solution degraded by different electrodes.

| | $RuO_2$-$TiO_2$/Ti electrode | La-doped $RuO_2$-$TiO_2$/Ti electrode |
|---|---|---|
| PA(%) | 70.33 | 75.61 |

electrode has lower $R_{ct}$ value than the undoped one, which indicates an increased electrochemical anodic reaction of oxygen formation at the film/solution interface. The UV irradiation results in the further lowering of $R_{ct}$ value.

The value of frequency independent n originating from Q [26] ranges between zero and unity. A value of zero corresponds to a pure resistor and a value of unity corresponds to a pure capacitor. The n value changes have been discussed by many researchers in literature in terms of diffusion phenomena, roughness, porosity, and pore size distribution [24]. Some authors have related the value with film rugosity: the higher the rugosity, the smaller the value of this parameter [27]. The La-doped electrodes have 0.62 and 0.66 of n lower than 0.73 or 0.75 of the undoped ones, which demonstrates a higher rugosity in microscale and is consistent with the SEM results.

The photogenerated holes in $TiO_2$ under UV irradiation could be trapped at the lattice oxygen and the trapped hole could be further transferred to an adsorbed water molecule, eventually producing oxygen [13,28]. The oxygen vacancies are the active sites for water dissociation and dye adsorption, as well as an origin of photoactivity under light [29]. To investigate the effect of La-doping on the amount of oxygen vacancies, the electron paramagnetic resonance (EPR) spectra are performed under UV irradiation as shown in Fig. 3. There are three major feature signals from photogenerated electrons and holes. The signals at g = 1.986 and 2.015 are assigned to surface hole trapping sites [18,30]. The remaining signals at g = 1.940 is the lattice electron trapping sites in rutile [31]. The coordinated bridging oxygen traps holes and forms $Ti^{4+}$–$O^{-}$–$Ti^{4+}$ and $Ti^{4+}$–$V_o$–$Ti^{4+}$ (here $V_o$ demonstrates oxygen vacancies) after further reduction by holes [28]. The EPR intensity originating from the surface hole trapping sites represents the amount of oxygen vacancies under UV irradiation. Curve (b) shows a much higher signal, which indicates that the doping of La is favorable to generate oxygen vacancies.

As one of the most important semiconductors, $TiO_2$ has drawn much attention due to its high photocatalytic activities to oxidize organics and waste water by producing photo-electrons and holes. $TiO_2$ doped with $La^{3+}$ ions has been found to improve the photoactivity on the degradation of organic molecules such as dye and other molecules hard to be degraded [32,33]. Table 2 gives the photodegradation rate of methylene solution degraded by different electrodes. La-doped $RuO_2$-$TiO_2$/Ti electrode shows 7.5% higher degradation rate under UV irradiation with low power density than that of the undoped $RuO_2$-$TiO_2$/Ti electrode. Recently, a lot of work has been successfully done in term of the computational studies to clarify the improved photocatalytic properties of high-content-La-doped $TiO_2$ films [18,34-36]. Zhao et. al find the changes in cell volume, bond length and charge on atoms due to the doping of La with larger ion radium result in the obvious increase in average dipole moments of $TiO_6$ and $LaO_6$. This greatly contributes to the separation of photoexcited electron–hole pairs. The formation energy of rutile $TiO_2$ [35] and oxygen vacancies [18] are also reported to decrease due to the doping of La ions. These are favorably to the enhancement of photocatalytic performance. The ratio of La dopant was another important factor and there was an optimal ratio of dopant [34]. In our experiment, we find there is higher density of oxygen vacancies probably due to the lower formation energy originating from the doping of La ions and larger number of cracks on the surface, and the increased conductivity. These factors may work together on the enhanced photoelectrochemical performance. A theoretical calculation and systematic investigation are being carried out to explain the enhanced degradation ability and mechanism resulting from the La-doping and UV irradiation.

## 4. Conclusions

The effect of La doping on the photoelectrochemical performance of DSA are investigated in this work. The doped electrodes prepared by thermal decomposition method show higher density of cracks in microscale on the electrode surface. They also present better photoelectrochemical activity than that of undoped ones. The electron paramagnetic resonance investigation shows the doping of La ions results in higher density of oxygen vacancies on the electrode surface. The increased electric conductivity and higher density of cracks and oxygen vacancies upon UV irradiation could be the reason that La-doped samples have better photoelectrochemical activities and 7.5% higher degradation rate of the methylene blue in aqueous solution.

## Declaration of Competing Interest

The authors declare that they have no known competing financial interests or personal relationships that could have appeared to influence the work reported in this paper.

## Acknowledgement

The authors would like to thank the financial support from the Guiding Project of Fujian Natural Science Foundation (No. 2019Y0047), Program for Innovative Research Team in Science and Technology in Fujian Province University and the Xiamen Municipal Science and Technology Project (No. 3502Z20179027).

## References

[1] C.A. Martinez-Huitle, E. Brillas, Decontamination of wastewaters containing synthetic organic dyes by electrochemical methods: a general review, Appl. Catal. B-Environ. 87 (2009) 105–145.
[2] R.K.B. Karlsson, H.A. Hansen, T. Bligaard, A. Cornell, L.G.M. Pettersson, Ti atoms in Ru0.3Ti0.7O2 mixed oxides form active and selective sites for electrochemical chlorine evolution, Electrochim. Acta. 146 (2014) 733–740.
[3] S. Trasatti, Electrocatalysis in the anodic evolution of oxygen and chlorine, Electrochim. Acta. 29 (1984) 1503–1512.
[4] S. Trasatti, Electrocatalysis: understanding the success of DSA®, Electrochim. Acta. 45 (2000) 2377–2385.
[5] K. Macounová, M. Makarova, J. Jirkovský, J. Franc, P. Krtil, Parallel oxygen and chlorine evolution on Ru1 − xNixO2 − y nanostructured electrodes, Electrochim. Acta. 53 (2008) 6126–6134.
[6] V. Petrykin, K. Macounová, M. Okube, S. Mukerjee, P. Krtil, Local structure of Co doped RuO2 nanocrystalline electrocatalytic materials for chlorine and oxygen evolution, Catal. Today 202 (2013) 63–69.
[7] V. Petrykin, K. Macounova, J. Franc, O. Shlyakhtin, M. Klementova, S. Mukerjee, P. Krtil, Zn-Doped RuO2 electrocatalyts for selective oxygen evolution: relationship between local structure and electrocatalytic behavior in chloride containing media,

Chem. Mater. 23 (2011) 200–207.
[8] S. Chen, Y. Zheng, S. Wang, X. Chen, Ti/RuO2–Sb2O5–SnO2 electrodes for chlorine evolution from seawater, Chem. Eng. J. 172 (2011) 47–51.
[9] J. Nowotny, W. Macyk, E. Wachsman, K.A. Rahman, Effect of Oxygen Activity on the n–p Transition for Pure and Cr-Doped TiO2, J. Phys. Chem. C 120 (2016) 3221–3228.
[10] R. Wang, K. Hashimoto, A. Fujishima, M. Chikuni, E. Kojima, A. Kitamura, M. Shimohigoshi, T. Watanabe, Light-induced amphiphilic surfaces, Nature 388 (1997) 431–432.
[11] R. Wang, K. Hashimoto, A. Fujishima, M. Chikuni, E. Kojima, A. Kitamura, M. Shimohigoshi, T. Watanabe, Photogeneration of highly amphiphilic TiO2 surfaces, Adv. Mater. 10 (1998) 135.
[12] R. Wang, N. Sakai, A. Fujishima, T. Watanabe, K. Hashimoto, Studies of surface wettability conversion on TiO2 single-crystal surfaces, J. Phys. Chem. B 103 (1999) 2188–2194.
[13] J. Zuo, E. Torres, Comparison of Adsorption of Mercaptopropyltrimethoxysilane on Amphiphilic TiO2 and Hydroxylated SiO2, Langmuir 26 (2010) 15161–15168.
[14] S. Saha, K. Kishor, R.G.S. Pala, Dissolution induced self-selective Zn- and Ru-doped TiO2 structure for electrochemical generation of KClO3, Catal. Sci. Technol. 8 (2018) 878–886.
[15] M. Xu, Z. Wang, F. Wang, P. Hong, C. Wang, X. Ouyang, C. Zhu, Y. Wei, Y. Hun, W. Fang, Fabrication of cerium doped Ti/nanoTiO2/PbO2 electrode with improved electrocatalytic activity and its application in organic degradation, Electrochim. Acta 201 (2016) 240–250.
[16] J. Xu, Y. Ao, D. Fu, C. Yuan, Study on photocatalytic performance and degradation kinetics of X-3B with lanthanide-modified titanium dioxide under solar and UV illumination, J. Hazard. Mater. 164 (2009) 762–768.
[17] J. Choi, H. Park, M.R. Hoffmann, Effects of single metal-ion doping on the visible-light photoreactivity of TiO2, J. Phys. Chem. C 114 (2010) 783–792.
[18] J. Zhang, Z. Zhao, X. Wang, T. Yu, J. Guan, Z. Yu, Z. Li, Z. Zou, Increasing the Oxygen Vacancy Density on the TiO2 Surface by La-Doping for Dye-Sensitized Solar Cells, J. Phys. Chem. C 114 (2010) 18396–18400.
[19] A.S. Weber, A.M. Grady, R.T. Koodali, Lanthanide modified semiconductor photocatalysts, Catal. Sci. Technol. 2 (2012) 683–693.
[20] Z.M. El-Bahy, A.A. Ismail, R.M. Mohamed, Enhancement of titania by doping rare earth for photodegradation of organic dye (Direct Blue), J. Hazard. Mater. 166 (2009) 138–143.
[21] Y. Murakami, T. Kondo, Y. Shimoda, H. Kaji, K. Yahikozawa, Y. Takasu, Effects of rare earth chlorides on the preparation of porous ruthenium oxide electrodes, J. Alloy. Compd. 239 (1996) 111–113.
[22] R. Shannon, Revised effective ionic radii and systematic studies of interatomic distances in halides and chalcogenides, Acta. Crystallographica Section A 32 (1976) 751–767.
[23] Z. Chen, J. Zhu, S. Zhang, Y. Shao, D. Lin, J. Zhou, Y. Chen, D. Tang, Influence of the electronic structures on the heterogeneous photoelectrocatalytic performance of Ti/RuxSn1-xO2 electrodes, J. Hazard. Mater. 333 (2017) 232–241.
[24] T.A.F. Lassali, J.F.C. Boodts, L.O.S. Bulhões, Charging processes and electrocatalytic properties of IrO2/TiO2/SnO2 oxide films investigated by in situ AC impedance measurements, Electrochim. Acta. 44 (1999) 4203–4216.
[25] J. Zuo, H. Wu, A. Chen, J. Zhu, M. Ye, J. Ma, Z. Qi, Shape-dependent photo-generated cathodic protection by hierarchically nanostructured TiO2 films, Appl. Surf. Sci. 462 (2018) 142–148.
[26] S. Kochowski, K. Nitsch, Description of the frequency behaviour of metal–SiO2–GaAs structure characteristics by electrical equivalent circuit with constant phase element, Thin Solid Films 415 (2002) 133–137.
[27] R.D. Armstrong, R.A. Burnham, The effect of roughness on the impedance of the interface between a solid electrolyte and a blocking electrode, J. Electroanal. Chem. Interfacial Electrochem. 72 (1976) 257–266.
[28] N. Sakai, A. Fujishima, T. Watanabe, K. Hashimoto, Quantitative evaluation of the photoinduced hydrophilic conversion properties of TiO2 thin film surfaces by the reciprocal of contact angle, J. Phys. Chem. B 107 (2003) 1028–1035.
[29] H.-H. Lo, N.O. Gopal, S.-C. Ke, Origin of photoactivity of oxygen-deficient TiO2 under visible light, Appl. Phys. Lett. 95 (2009) 083126.
[30] O.I. Micic, Y. Zhang, K.R. Cromack, A.D. Trifunac, M.C. Thurnauer, Trapped holes on titania colloids studied by electron paramagnetic resonance, J. Phys. Chem. 97 (1993) 7277–7283.
[31] D.C. Hurum, A.G. Agrios, S.E. Crist, K.A. Gray, T. Rajh, M.C. Thurnauer, Probing reaction mechanisms in mixed phase TiO2 by EPR, J. Electron Spectrosc. Relat. Phenom. 150 (2006) 155–163.
[32] S.J. Armaković, M. Grujić-Brojčin, M. Šćepanović, S. Armaković, A. Golubović, B. Babić, B.F. Abramović, Efficiency of La-doped TiO2 calcined at different temperatures in photocatalytic degradation of β-blockers, Arabian J. Chem. (2017).
[33] M. Grujić-Brojčin, S. Armaković, N. Tomić, B. Abramović, A. Golubović, B. Stojadinović, A. Kremenović, B. Babić, Z. Dohčević-Mitrović, M. Šćepanović, Surface modification of sol–gel synthesized TiO2 nanoparticles induced by La-doping, Mater. Charact. 88 (2014) 30–41.
[34] L. Bian, M. Song, T. Zhou, X. Zhao, Q. Dai, Band gap calculation and photo catalytic activity of rare earths doped rutile TiO2, J. Rare Earths 27 (2009) 461–468.
[35] Y. Xin, H. Liu, Study on mechanism of photocatalytic performance of La-doped TiO2/Ti photoelectrodes by theoretical and experimental methods, J. Solid State Chem. 184 (2011) 3240–3246.
[36] Z. Zhao, Q. Liu, Effects of lanthanide doping on electronic structures and optical properties of anatase TiO2from density functional theory calculations, J. Phys. D Appl. Phys. 41 (2008) 085417.